NEOPLASIA
www.neoplasia.com
Volume 23 Number xxx Month 2021 pp. 594–607

Original Research

Lysyl hydroxylase 2-induced collagen cross-link switching promotes metastasis in head and neck squamous cell carcinomas ☆

Kotaro Sato [a,b,c,1]; Kshitij Parag-Sharma [d,1]; Masahiko Terajima [c]; Adele M. Musicant [b,c]; Ryan M. Murphy [3]; Matthew R. Ramsey [f]; Hideharu Hibi [a]; Mitsuo Yamauchi [c,*]; Antonio L. Amelio [c,g,h,i,2,*]

[a] Department of Oral and Maxillofacial Surgery, Graduate School of Medicine, Nagoya University, Nagoya, Japan
[b] Lineberger Comprehensive Cancer Center, UNC School of Medicine, The University of North Carolina at Chapel Hill, NC, USA
[c] Division of Oral and Craniofacial health Sciences, Adams School of Dentistry, The University of North Carolina at Chapel Hill, NC, USA
[d] Graduate Curriculum in Cell Biology & Physiology, Biological & Biomedical Sciences Program, UNC School of Medicine, The University of North Carolina at Chapel Hill, NC, USA
[3] Graduate Curriculum in Pharmacology, Biological & Biomedical Sciences Program, UNC School of Medicine, The University of North Carolina at Chapel Hill, NC, USA
[f] Department of Dermatology, Brigham and Women's Hospital, Harvard Medical School, Boston, MA, USA
[g] Department of Cell Biology and Physiology, UNC School of Medicine, University of North Carolina at Chapel Hill, Chapel Hill, NC, USA
[h] Biomedical Research Imaging Center, UNC School of Medicine, The University of North Carolina at Chapel Hill, NC, USA
[i] Lineberger Comprehensive Cancer Center, Cancer Cell Biology Program, UNC School of Medicine, University of North Carolina at Chapel Hill, Chapel Hill, NC, USA

Abstract

Head and neck squamous cell carcinoma (HNSCC) is the 6th most common cancer worldwide and incidence rates are continuing to rise globally. HNSCC patient prognosis is closely related to the occurrence of tumor metastases, and collagen within the tumor microenvironment (TME) plays a key role in this process. Lysyl hydroxylase 2 (LH2), encoded by the Procollagen-Lysine,2-Oxoglutarate 5-Dioxygenase 2 (*PLOD2*) gene, catalyzes hydroxylation of telopeptidyl lysine (Lys) residues of fibrillar collagens which then undergo subsequent modifications to form stable intermolecular cross-links that change the biomechanical properties (i.e. quality) of the TME. While LH2-catalyzed collagen modification has been implicated in driving tumor progression and metastasis in diverse cancers, little is known about its role in HNSCC progression. Thus, using gain- and loss-of-function studies, we examined the effects of LH2 expression levels on collagen cross-linking and cell behavior *in vitro* and *in vivo* using a tractable bioluminescent imaging-based orthotopic xenograft model. We found that LH2 overexpression dramatically increases HNSCC cell migratory and invasive abilities *in vitro* and that LH2-driven changes in collagen cross-linking robustly induces metastasis *in vivo*. Specifically, the amount of LH2-mediated collagen cross-links increased significantly with *PLOD2* overexpression, without affecting the total quantity of collagen cross-links. Conversely, LH2 knockdown significantly blunted HNSCC cells invasive capacity *in vitro* and metastatic potential *in vivo*. Thus, regardless of the total "quantity" of collagen crosslinks, it is the "quality" of these cross-links that is the key driver of HNSCC tumor metastatic dissemination. These data implicate LH2 as a key regulator of HNSCC tumor invasion and metastasis by

* Corresponding author.
E-mail addresses: antonio-amelio@unc.edu, alamelio@email.unc.edu (A.L. Amelio).
☆ *Abbreviations*: ECM, extracellular matrix; HNSCC, head and neck squamous cell carcinoma; LOX, lysyl oxidase; PLOD2, Procollagen-Lysine,2-Oxoglutarate 5-Dioxygenase 2.
[1] These authors contributed equally
[2] Twitter handle: @AmelioLab.
Received 25 March 2021; received in revised form 19 May 2021; accepted 21 May 2021

https://doi.org/10.1016/j.neo.2021.05.014

modulating collagen cross-link quality and suggest that therapeutic strategies targeting LH2-mediated collagen cross-linking in the TME may be effective in controlling tumor progression and improving disease outcomes.

Neoplasia (2021) 23, 594–607

Keywords: Head and neck cancer, Extracellular matrix, Collagen Cross-linking, Lysyl hydroxylase 2, Procollagen-Lysine,2-Oxoglutarate 5-Dioxygenase 2, Metastasis

Introduction

Head and neck squamous cell carcinomas (HNSCC) are the sixth leading cancer by incidence worldwide with an estimated 600,000 new cases per year [4, 10, 24]. In the United States, HNSCC accounts for ∼3% of all cancers with an estimated 54,000 new cases and 11,000 deaths per year [52]. More than half of these new cases involve patients diagnosed with advanced stage disease that is associated with poor prognosis and low 5-y survival rates [51]. The frequent emergence of local disease recurrence and tumor metastasis contributes to the high morbidity and mortality associated with this cancer [46]. Notably, HNSCCs often exhibit desmoplastic features characterized by excessive accumulation of fibrillar collagen within the stroma that forms a stiff extracellular matrix (ECM) [26]. The progressive linearization and thickening of collagen is known to augment cell growth and survival, via cellular mechanosignaling [29, 39], and lead to increased cell migration and metastatic progression [28, 37].

Fibrillar type I collagen is the major component of the tumor stroma in solid cancers [16, 27, 55]. Type I collagen is a heterotrimeric molecule composed of 2 α1 chains and one α2 chain, which consist of 3 structural domains: Amino-terminal nonhelical telopeptide (N-telo), central triple helix (helical), and carboxy-terminal nonhelical telopeptide (C-telo) domains [63]. After procollagen molecules are synthesized and post-translationally modified within cells, they are secreted into the extracellular space and undergo additional enzymatic processing before self-assembling into a fibril, which is then stabilized by covalent intermolecular cross-linking [62]. Cross-linking is initiated by the conversion of telopeptidyl lysine (Lys) and hydroxylysine (Hyl) to the respective aldehyde, Lys^{ald} and Hyl^{ald}, via the action of lysyl oxidase (LOX) and LOX-like enzymes (LOXL1-4). These aldehydes then undergo a series of condensation reactions involving the juxtaposed Lys, Hyl and histidine (His) residues on the neighboring collagen molecules. The critical feature that determines the stability of cross-links is the state of Lys hydroxylation in telopeptides; Hyl^{ald}-derived cross-links are more stable in comparison to Lys^{ald}-derived cross-links [8, 20, 61]. The Lys hydroxylation reactions are catalyzed by lysyl hydroxylases 1-3 (LH1-3). However, only LH2, encoded by the Procollagen-Lysine,2-Oxoglutarate 5-Dioxygenase 2 (*PLOD2*) gene (LH2 hereafter), catalyzes Lys hydroxylation specifically within the *N*- and *C*-telopeptides [45, 58, 60].

Recent studies have shown that aberrant collagen cross-linking plays a significant role in controlling tumor ECM stiffness, which promotes cancer progression and metastasis [9, 28, 48, 62]. Thus, much attention has been paid to the role that collagen modifying enzymes such as LOX family members and LH2 play in determining the quantity and quality of collagen cross-linking, respectively. It has been reported that LOX and LOXL2 are widely up-regulated in tumors [1, 11, 32], suggesting that the overall quantity of collagen cross-links is increased across many cancers. More recent reports have shown that LH2 is specifically up-regulated in late-stage, metastatic cancers [9, 14, 19, 48], strongly suggesting that a 'switch' in tumor-ECM quality resulting from LH2-mediated stable Hyl^{ald}-derived cross-links drives aggressive tumor behaviors. Taken together, it is now abundantly clear that the biomechanical nature of fibrillar collagens plays a critical role in modulating cancer cell behaviors associated with migration and metastasis [25, 41, 62]. However, little is known about the functional role of LH2 in the pathobiology of HNSCC maintenance and/or progression.

In this study, we mechanistically examined the effects of LH2 expression levels on collagen cross-linking, and specifically how these modifications affect tumor cell behavior, both *in vitro* and *in vivo,* using tractable HNSCC models. Using both gain- and loss-of-function studies we report that LH2 is a key regulator of HNSCC cell migration, invasion and lymph node metastasis and that stable LH2-modified collagen cross-links are both necessary and sufficient to augment these invasive behaviors and promote metastatic dissemination.

Materials and methods

Cell culture

All cell lines used in this study are of human origin. "Normal" immortalized keratinocyte cell lines OKF4-TERT and OKF6-TERT cells were kindly provided by Drs. Jim Rheinwald and Matthew Ramsey at Harvard University [13] and cultured in Keratinocyte Serum Free media (KSFM media; Gibco, cat#; 17-005-042) supplemented with 25 ug/mL of Bovine pituitary extract (Sigma-Aldrich, cat#; P1167-5MG) + 1x Penicillin-Streptomycin-Glutamine (PSG; Thermo fisher, cat#; 10378-016) + 0.2 ng/mL Epithelial Growth Factor (Sigma-Aldrich, cat#; E9644) + 0.3 mM Calcium Chloride. The GMSM-K normal immortalized keratinocyte cell line was kindly provided by Dr. Valerie Murrah at the University of North Carolina-Chapel Hill [18] and cultured in KSFM supplemented with 50 ug/mL of Bovine pituitary extract + 1x Penicillin-Streptomycin-Glutamine + 50 ng/mL Epithelial Growth Factor. The UM-SCC-5, UM-SCC-11A, UM-SCC-14A, and UM-SCC-74A cells were kindly provided by Dr. Thomas Carey at the University of Michigan-Ann Arbor [5] and cultured in Dulbecco's modified Eagle's medium (Gibco, cat#; 11965-118) supplemented with 10% Heat-inactivated Fetal Bovine Serum (Atlanta Biologicals, cat#: S11550) + 1x Glutamax (Gibco, cat#; 35050061) + 1x Nonessential amino acids (Gibco, cat#; 11140050) + 1x PSG. The FBS was heat inactivated by a 30-min incubation at 55°C. The UM-SCC-15 and UM-SCC-25 cells, also obtained from Dr. Thomas Carey at the University of Michigan-Ann Arbor [5], were cultured in DMEM/F12 medium (Gibco, cat#; 11320033) supplemented with 10% FBS + 15 mM HEPES (Corning, cat#; 25-060-CI) + 0.5 mM Sodium Pyruvate (LifeTech, cat#; 11360070) + 400 ng/mL Hydrocortisone (Sigma-Aldrich, cat#: H0888). The UM-SCC-47, UM-SCC-2, SCC-090 and 93-VU-147T cells were kindly provided by Dr. Randall Kimple at the University of Wisconsin and cultured in DMEM supplemented with 10% Fetal Bovine Serum + 1x Glutamax + 1x PSG. STR profiling (LabCorp DNA Identity) were performed on the OKF6-TERT, UM-SCC-5, and UM-SCC-74A cell lines to confirm their authenticity.

qPCR

RNA was isolated using the NucleoSpin RNA kit (Macherey-Nagel, #740955) following the manufacturer's protocol. RNA was eluted in RNase-free water and quantified using a Cytation 5 plate multimode reader spectrophotometer. cDNA was synthesized using the iScript cDNA Synthesis Kit (BioRad cat, #: 170-8891). Quantitative RT-PCR was performed using FastStart Universal SYBR Green Master (Roche cat, #: 04913850001), using 2 µL of cDNA (10 ng/µL) per reaction. qPCR primers used were as follows:

LH1:
sense: 5'-GAGCAGCATCCCTCGTTTCT-3'
antisense: 5'-AACTGAGCTGAGCGCTTGAA-3'
endogenous LH 2:
sense: 5'-CTCCCAAAGCTAAGTGCAGG-3'
antisense: 5'-TCAGCGCGGACGCTATTT-3'
exogenous ly overexpressed LH 2:
sense: 5'-GACCCGAGGAAGTGCTGAAG-3'
antisense: 5'-CTTGTCGGCCAGTCTCTTGT -3'
LH3:
sense: 5'-ATACGCTGACCGGGAGGATA-3'
antisense: 5'-CTGCCACTCTGGACGAACTT-3'
LOX:
sense: 5'-CCTACTACATCCAGGCGTCC-3'
antisense: 5'-GCCCTGTATGCTGTACTGGC-3'
LOXL2:
sense: 5'-CACCTGCGAGAATGGGCTAC-3'
antisense: 5'-GGGGTTGCTCTGGCTTGTA-3')
RPL23:
sense: *5'*-TGATGGCCACAGTCAAGAAA-*3'*
antisense: 5'-ACACGCCATCTTTTCTACGG-*3'.*

LH2 isoform-specific PCR

mRNA was extracted from GMSMK, UMSCC-5 and UMSCC-74A cells using the NucleoSpin RNA kit (Macherey-Nagel, #740955) following the manufacturer's protocol. RNA was eluted in RNase-free water and quantified using a Cytation 5 plate multimode reader spectrophotometer. cDNA was synthesized using the SuperScript IV Synthesis Kit (BioRad cat, #: 170-8891) using oligo-dT primers. LH2 was amplified via PCR using previously validated and published isoform-specific primers and quantified as described [21].

LH 2 a versus LH2b isoform:
sense: 5'-CGATCAGAGATGAATGAAAGG-3'
antisense: 5'-GCAGTGGATAATAGCCTTCC-3'

Western blotting

Cells were lysed (250 mM NaCl, 50 mM Tris pH7.4, 50 mM NaF, 0.1 mM NaVO4, 5 mM EDTA, 0.1% triton-X, and protease and phosphatase inhibitors) and total protein concentration was quantified by BCA assay (Thermo Scientific, cat#; 23225). SDS-PAGE electrophoresis was performed using ~20 µg protein. Blots were incubated with primary antibodies diluted in 5% skim milk/TBST overnight at 4°C. Horseradish peroxidase-conjugated secondary antibody (#7074, Cell Signaling Technology, USA) was diluted 1:10,000 in 5% skim milk/TBST and incubated for 1 h at room temperature. Protein bands were visualized using Clarity Western ECL Substrate (Bio-Rad, USA) and analyzed with ImageJ 4.7v software (National Institutes of Health, Bethesda, MD, USA). anti-LH2 polyclonal antibody (1:100 dilution, Proteintech Group, USA), β-actin (1:10000 dilution, Sigma-Aldrich, USA).

Wound healing assay

Cells were seeded in a 6 well plate in media with or without 1 µg/mL doxycycline and cultured for 3 d (UM-SCC-5) or 7 d (UM-SCC-74A) to ensure maximal overexpression/knockdown, respectively. Wells were washed and fresh media/Dox added daily. Cells were then trypsinized, counted and seeded for the wound healing assay. Ibidi 2 well culture inserts (Ibidi, cat#; 81176) were placed in a 24 well dish and cells were seeded (UM-SCC-5= 100,000 per side and UM-SCC-74A= 30,000 per side) in a 100 µL volume on each side of the insert. 24 h postseeding, once cells had formed a 100% confluent monolayer, the Ibidi culture inserts were gently and carefully removed from the wells. Wells were washed once with 1xDPBS and 1 mL of fresh media with/without doxycycline was added. Wound healing/scratch closing was imaged once every hour over a period of 24 h using a Cytation 5 plate imager (BioTek Instruments, Inc). Three independent fields of view were imaged per well for each biologic replicate. Wound size was quantified manually using the area measurement function in ImageJ software.

Transwell Matrigel Invasion Assay (Boyden chamber)

Cells were seeded in a 6 well plate in media with or without 1 µg/mL doxycycline. Cells were cultured for 2 d (UM-SCC-14A), 3 d (UM-SCC-5) or 7 d (UM-SCC-74A) to ensure maximal overexpression/knockdown, respectively. Wells were washed and fresh media/Dox added daily. Cells were then trypsinized, washed, counted, and resuspended in low-serum media (regular culture media without FBS, supplemented with 0.1% BSA). Prior to seeding cells onto the transwell chamber (Falcon permeable-transwell chambers- 8 um pore membrane, cat#; 353097), the transwell membrane was first coated with 5 % Matrigel (Corning, cat#; 356234). Briefly, 100 µL of 5 % Matrigel solution was added to the transwell chamber, which was then incubated for 1 h in a humidified 37C, 5% CO_2 cell culture incubator to ensure polymerization. Postpolymerization, the transwell chamber was placed in a 24 well plate well containing 750 µL of complete UM-SCC cell culture media (chemoattractant). Cells were seeded (UM-SCC-5 = 500,000/transwell, UM-SCC-14A = 125,000/transwell, or UM-SCC-74A = 100,000/transwell) into the transwell chamber in 1 mL of low-serum media and allowed to invade through the Matrigel and onto the bottom side of the transwell membrane for 24 h. Twenty-four hours postseeding, cells were fixed using 10% formalin, 5 min at room temperature. Cells were visualized using 0.05% crystal violet, 30 min incubation at room temperature followed by 5 washes using distilled water. Noninvaded cells still adhered to the 'top-side' of the transwell chamber were removed using cotton swabs. Membranes were dried overnight, and invaded cells were imaged in brightfield using a Cytation 5 plate imager. In order to accurately quantify the number of fully invaded cells, we sought to quantify the number of nuclei, instead of performing the quantification based solely on the crystal violet staining. Cells were de-stained by incubating in 1% Triton-X100 for 45 min at room temperature. Nuclei were stained with DAPI (0.5 μM in 1xDPBS, for 15 min) and imaged using a Cytation 5 plate imager. Number of nuclei was counted across at least 5 random fields of view using the Cell Counter plugin in ImageJ software.

Plasmids

The pRRL-rtTA3 lentiviral vector was kindly provided by J. Zuber, Research Institute of Molecular Pathology, Vienna, Austria, TRE-KRAB-dCas9-IRES-BFP was a gift from Eric Lander (Addgene plasmid # 85449), pgRNA-CKB vector for guide RNA expression was a gift from Bruce Conklin (Addgene plasmid # 73501), and Hs-LH2 plasmid was a gift from Gavin Wright (Addgene plasmid # 51756).

Doxycycline-inducible LH2 *retrovirus cloning*

Generating the RetroX-TRE3G::MCS_PGK::GpNLuc vector

First, the 2nd generation pTight promoter from the RetroX-pTight::MCS_PGK::GpNLuc (Addgene plasmid # 70185) was replaced with a 3rd generation doxycycline response promoter; TRE3G. Briefly, the pTight promoter was excised using BamHI/XhoI restriction enzymes (New England Biosciences, cat#; R3136 and R0146, respectively). The BamHI digested vector was blunted using T4 polymerase (NEB, cat#; M0203) prior to the XhoI digestion in order to generate a blunt end/sticky end vector backbone. The dually digested plasmid was run in a 1% agarose gel and the digested backbone fragment (~7150 bp) was excised and purified (Macherey-Nagel PCR clean up kit, cat. #: 740609). Next, the TRE3G promoter was excised from a previously published plasmid (TRE-KRAB-dCas9-IRES-BFP, Addgene plasmid # 85449) using SmaI/XhoI restriction enzymes (NEB, cat#; R0141). The digested vector backbone and insert, 1:6 ratio, were ligated overnight using T4 DNA ligase (NEB, cat#; M202) and transformed into homemade (Zymo Research, cat#; T3001) chemically competent E.coli Stable3 cells (NEB, cat#; C304). Multiple clones were miniprepped (Macherey-Nagel NucleoSpin kit, cat. #: 740588) and sequence verified (Eton Biosciences, Inc). All enzyme incubations were performed in accordance with the manufacturer's recommendations.

Generating the RetroX-TRE3G::HsLH2-T2A-Hygromycin_PGK::GpNLuc vector

The newly generated and sequence verified RetroX-TRE3G::MCS_PGK::GpNLuc vector was digested and dephosphorylated using BamHI/EcoRI (NEB, cat#; R3136 and R3101, respectively) and recombinant Shrimp Alkaline Phosphatase (NEB, cat#; M0371). The digested/dephosphorylated plasmid was column purified (Macherey-Nagel PCR clean up kit, cat. #: 740609). The *LH2* cDNA insert was PCR amplified from a previously published vector (Addgene plasmid # 51756) [53] using Pfu Ultra DNA polymerase (Agilent, cat. #: 600380), and simultaneously, restriction enzyme sites 5'-BamHI-*LH2*-XbaI-3' were added into the amplicon using the PCR primers (*sense = 5'-ctcctcGGATCCgcggccgccaccatgg-3'* + *antisense = 5'-ctcctcTCTAGAcgcgccagggtcgatgaag-3'*). The T2A-Hygromycin insert was PCR amplified from a previously published vector (Addgene plasmid # 154263) [35], and simultaneously, restriction enzyme sites 5'-XbaI-T2A-Hygromycin-EcoRI-3' were added into the amplicons using the PCR primers (*sense = 5'- CTCCTCtctagaATGGACGAGCTGTACAAGGGCT-3'* + *antisense = 5'- CTCCTCgaattcCTATTCCTTTGCCCTCGGACGAG-3'*). The PCR amplicons were run in a 1% agarose gel and the appropriate bands (*LH2* = 2220 bp and T2A-Hygromycin= 1120 bp) were excised and purified. The PCR amplicons were digested with BamHI/XbaI or XbaI/EcoRI as indicated (NEB, XbaI-cat#; R0145), and the digestion reaction was column purified. The digested/dephosphorylated backbone and digested PCR amplicon inserts were ligated, 1:3:3 ratio, using T4 DNA ligase overnight and transformed into homemade chemically competent E.coli Stable3 cells. Multiple clones were miniprepped and sequence verified (Eton Biosciences, Inc). All enzyme incubations were performed in accordance with the manufacturer's recommendations. These vectors have been deposited with Addgene (https://www.addgene.org/Antonio_Amelio/).

Design and cloning of PLOD2 *gene promoter-targeting guide RNAs*

PLOD2 guide RNA design

sgRNA for knocking down *PLOD2* using CRISPR-interference (dCas9-KRAB) were designed using the CRISPR-ERA resource (http://crispr-era.stanford.edu/). The top 3 guide RNA sequences were cloned (see below) and validated for *PLOD2* knockdown efficiency by qPCR and Western blotting.

PLOD2 *targeting sgRNA 3*
sense: 5'-TCAGCCGGCGGCCAATAGCC-3'
PLOD2 targeting sgRNA 4
sense: 5'-TGAGCAAACAGTCCAGACGT-3'
PLOD2 targeting sgRNA 5
sense: 5'-CTGAGCAAACAGTCCAGACG-3'

PLOD2 targeting guide RNA cloning

The pgRNA-CKB vector (Addgene plasmid # 73501) was used to constitutively express the guide RNAs. Guide RNAs were cloned into the pgRNA-CKB vector using previously published methods [30]. Briefly, pgRNA-CKB backbone was digested with Esp3I (NEB, cat#; R0734) and dephosphorylated using recombinant Shrimp Alkaline Phosphatase. The required guide RNAs were synthesized (Eton Biosciences, Inc) as oligonucleotides with Esp3I compatible overhangs (forward oligo overhang = 5'-TTGG—sgRNA, reverse oligo overhang = 5'-AAAC—sgRNA). Oligonucleotides (50 µL reaction, 2 µM Forward/Reverse oligo final) were phosphorylated using T4 Poly Nucleotide Kinase (NEB, cat#; M0201) and annealed. Annealing was performed by adding 50 µM sodium chloride to the phosphorylated oligo reaction, denaturing the oligo mix via boiling (95°C for 10 min) followed by an extended, slow cooling step (~0.1°C/sec). The annealed and phosphorylated sgRNAs were diluted to a final concentration of 0.1 µM. 100 ng of the digested/dephosphorylated pgRNA-CKB backbone was ligated with 1 µL of the 0.1 µM phosphorylated/annealed guide RNA oligos using T4 DNA ligase overnight and transformed into homemade chemically competent E. coli Stable3 cells. Multiple clones were miniprepped and sequence verified (Eton Biosciences, Inc) using a 5'- gagatccagtttggttagtaccggg-3' sequencing primer. All enzyme incubations were performed in accordance with the manufacturer's recommendations. The various pgRNA-CKB-PLOD2 guide RNA vectors described in this study have been deposited with Addgene (https://www.addgene.org/Antonio_Amelio/).

Viral transductions (spinfection)

All virus transductions were performed using established spinfection protocols. Briefly, cells were seeded in 6 well/24 well plates. Twenty-four hours postseeding, wells were washed and fresh media was added (1.5 mL/500 µL respectively). The required virus was diluted into fresh media (500 µL/250 µL respectively) and polybrene was added to a final concentration of 4 µg/mL. Virus/polybrene mixture was gently mixed and added dropwise onto the cells. Plates were spinfected by centrifugation at 1200 g for 1.5 h at 30°C (Sorvall LYNX 4000, Thermo Scientific, cat#; 75006580). Plates were returned to a humidified 5% CO_2, 37°C cell culture incubator post spinfection. Cells were supplemented with 1 mL of fresh media 48 h postspinfection. Cells were split 72 h postspinfection and expanded for downstream applications (selection/FACS).

Generation and validation of doxycycline inducible LH2 overexpression cells

UM-SCC-5 and UM-SCC-14A cells were first transduced with a lentivirus encoding the doxycycline-responsive reverse tetracycline transactivator 3 protein ($rtTA^3$). $rtTA^3$ is constitutively expressed from this vector under the control of the EF1a promoter. A positively transduced polyclonal population was obtained by applying a puromycin antibiotic selection and rtTA3 mRNA expression was confirmed via real-time PCR. Next, these cells were transduced via spinfection with the retrovirus containing the doxycycline inducible *LH2* and constitutively expressed GpNLuc LumiFluor cassette (see above for TRE3G:LH2 plasmid cloning information). A positively transduced polyclonal population was obtained by FACS selection. Untransduced cells were used as a GFP-negative gating controls.

The doxycycline induced *LH2* overexpression was validated at both mRNA and protein levels. Cells were doxed (125 ng/mL-2 mg/mL doxycycline) over a period of 72 h, with fresh doxycycline added daily. Cells were harvested for mRNA (NucleoSpin RNA kit (Macherey-Nagel, cat#; 740955)) and protein (RIPA buffer- [150 mM sodium chloride, 1.0% NP-40, 1.0% sodium deoxycholate, 0.1% sodium dodecyl sulfate, 25 mM Tris, pH 7.6, 20 mM NaF, 1 MM EDTA, supplemented with protease inhibitors (cOmplete, EDTA-free Protease Inhibitor Cocktail - Roche, cat. #; 04693132001) and phosphatase inhibitors (phosphoSTOP, - Roche, cat. #; 10917400)]). Unmodified 'parental' UM-SCC-74A and UM-SCC-5 cells were used as positive/negative controls (high/low expressor, respectively).

Generation and validation of doxycycline inducible LH2 knockdown cells

Stable CRISPRi (dCas9-KRAB) UM-SCC-74A cells were generated by first transducing cells with a previously published lentivirus encoding constitutively expressed GpNLuc Lumifluor and puromycin selection cassettes (Addgene plasmid # 135935). A positively transduced polyclonal population was obtained by applying puromycin to the cells for 14 d. Next, these GpNLuc positive cells were simultaneously transduced with 2 additional lentiviruses, (1) encoding the doxycycline-responsive reverse tetracycline transactivator 3 protein (rtTA^3), constitutively expressed via an EF1a promoter, and (2) encoding the doxycycline induced dCas9-KRAB-IRES-BFP (Addgene plasmid # 85449) cassettes. Since the BFP protein is under the control of the doxycycline-responsive TRE3G promoter, only cells dually transduced with both rtTA^3 and dCas9-KRAB-IRES-BFP viruses will express BFP upon doxycycline treatment. Thus, transduced triple positive cells were selected by applying doxycycline treatment for 72 h, followed by FACS selection for the GFP+ve/BFP+ve cell population, and single GpNLuc stable cells were used as gating controls. Lastly, these triple positive UM-SCC-74A cells (GpNLuc/rtTA^3/dCas9-KRAB) were transduced with lentiviruses encoding the *LH2* targeting sgRNAs of interest. These *LH2* targeting sgRNAs expression vectors were generated from a previously published guide RNA vector (Addgene plasmid # 73501), which also contains a constitutively expressed 2xNLS-mKate2 fluorescent reporter and blasticidin antibiotic resistance cassettes. Positively transduced cells were selected via blasticidin antibiotic selection. The quadruple positive stable cells (GpNLuc/rtTA^3/dcas9-KRAB/guide RNA) were confirmed by fluorescent microscopy as being positive for GFP, BFP (doxycycline induced) and nuclear mKate2.

The doxycycline induced LH2 knockdown was validated at both mRNA and protein levels. Cells were doxed for 7 d with 1 μg/mL doxycycline, with fresh doxycycline added daily. Cells were harvested for mRNA (NucleoSpin RNA kit, Macherey-Nagel, cat#; 740955) and protein (RIPA buffer [150 mM sodium chloride, 1.0% NP-40, 1.0% sodium deoxycholate, 0.1% sodium dodecyl sulfate, 25 mM Tris, pH 7.6, 20 mM NaF, 1 MM EDTA, supplemented with protease inhibitors (cOmplete, EDTA-free Protease Inhibitor Cocktail, Roche; cat.# 04693132001) and phosphatase inhibitors (phosphoSTOP, Roche, cat#; 10917400)]). Unmodified UM-SCC-74A and UM-SCC-5 cells were used as positive/negative controls (high/low expressor, respectively)

In vivo orthotopic xenograft

Female nude mice (6–10 wk old) were injected with 10^5 trypsin-dissociated single cells in a total volume of 30 μL (15 μL Hanks Balanced Salt Solution + 15 μL Matrigel) into the left lateral tongue. Mice were kept anesthetized during the procedure (2–2.5% isoflurane gas). Doxycycline was administered via chow (1000 ppm Doxy Diet, Envigo, cat# TD.180096). Animals in the Dox cohort were prefed Dox chow for 3 d prior to orthotopic implantation and subsequently maintained on the Dox chow diet for the course of this experiment. Endpoint was determined by a more than 20% loss of their maximum body weight or if the animals had become moribund. To determine tumor volume by external caliper, the greatest longitudinal diameter (length) and the greatest transverse diameter (width) were determined. We defined tumor volume as 1/2(length × width^2). Consequently, lymph nodes, submaxillary gland, lung and liver were harvested and placed into 12 or 24 well plate to perform *ex vivo* analysis. This research was approved by The University of North Carolina at Chapel Hill Institutional Animal Care and Use Committee (Protocol No.17-202).

In vivo longitudinal bioluminescent imaging

Bioluminescent-fluorescent BRET signal was quantified noninvasively as previously described [49] with slight modifications. Briefly, animals were i.p. injected with 250 μM (1:20 dilution, ~500 μg/kg) Nano-Glo Luciferase Assay Substrate (Promega, cat. #N1120) in sterile DPBS. Isoflurane-anesthetized (3%) animals were imaged using the AMI Optical Imager (Spectral Instruments Imaging, Inc.) 5 min after injection. Mice were imaged using the following camera settings: Exposure time= 5 min, Binning= Medium, *F*-stop= 1.2, Field of view= 25. Data were analyzed using the Aura software package (https://spectralinvivo.com/software/).

Collagen biochemical analysis

After harvesting tongue tumors from each mouse, tissues were pulverized in liquid nitrogen, washed with cold PBS and distilled water, and lyophilized. Dried samples (~3.0 mg each) were reduced with standardized NaB^3H_4, hydrolyzed with 6N HCl and subjected to amino acid and cross-link analyses as previously reported [64]. Collagen composition (% of collagen in total proteins) was determined based on the value of 100 hydroxyproline (Hyp) residues per 1000 total amino acids in collagen. The level of Hyl per collagen was determined by Hyl/HypX300. The reducible cross-links, i.e. dehydrodihydroxylysinonorleucine/its ketoamine (deH-DHLNL), dehydrohydroxylysinonorleucine/its ketoamine (deH-HLNL) and dehydrohistidinohydroxymerodesmosine (deH-HHMD) were analyzed as their reduced forms, i.e. DHLNL, HLNL, and HHMD, respectively. The nonreducible, stable cross-links, pyridinoline (Pyr) and deoxypyridinoline (d-Pyr), were simultaneously analyzed by their specific fluorescence. The total number of aldehydes was calculated as DHLNL + HLNL + 2 × Pyr + 2 × d-Pyr + 2 × HHMD and the ratio of Hyl^{ald}- derived collagen cross-links (HLCCs) to Lys^{ald} derived collagen cross-links (LCCs) was calculated as (DHLNL+ Pyr + d-Pyr)/HHMD as previously reported [9].

Histological analysis

Harvested tissues were fixed in 10% buffered formalin solution for at least 72 hrs. Following fixation, tissues were processed on an ASP6025 automated tissue processor (Leica Biosystems). Paraffin embedded tissue blocks were sectioned at 5 μm, mounted on glass slides, and deparaffinized prior to Hematoxylin and Eosin (H&E) staining. Immunohistochemistry was performed on the Discovery Ultra (Ventana Medical Systems) using manufacturer's reagents. For LH2 immunohistochemistry, anti-LH2 (Proteintech #21214-1-AP) was prepared using Discovery PSS Diluent (cat. #: 760-212). Antigen retrieval was performed using Ventana's CC1 (pH 8.5) for 64 min at 90°C and slides were given a hydrogen peroxide block for 8 min at room temperature. Slides were then incubated in the primary antibody diluent (1:50) for 1 h at room temperature, followed by anti-Rabbit HRP secondary antibody for 32 min at room temperature.

Picrosirius red staining was performed to visualize collagen fibers as previously described [33, 48]. Briefly, FFPE sections were stained with Hematoxylin (Sigma-Aldrich, cat#; MHS32-1L) to visualize cell nuclei. Then, 0.1% Sirius red stain (Electron Microscopy Sciences, cat#; 26357-02), dissolved in saturated picric acid, was applied to FFPE sections for 1

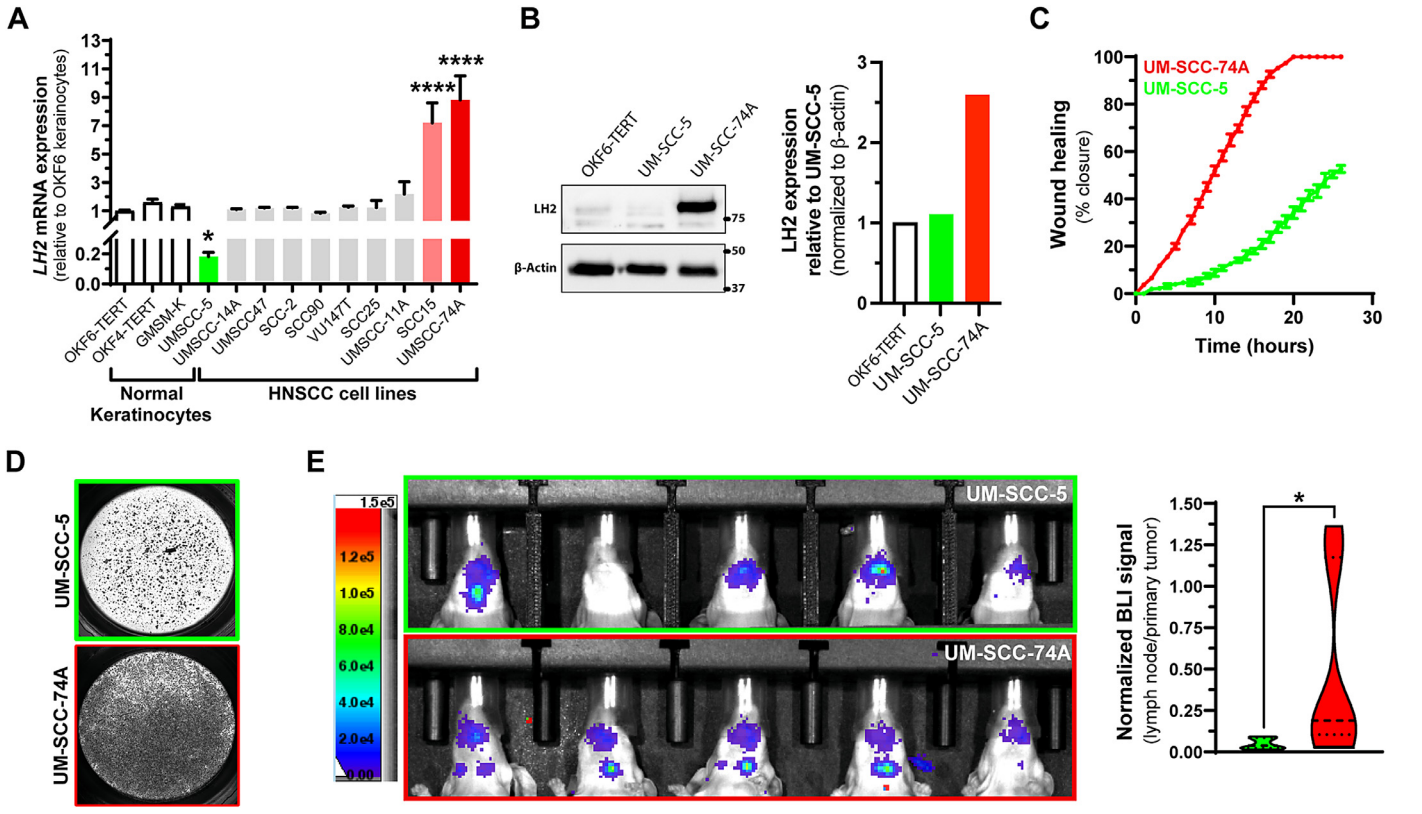

Fig. 1. LH2 expression levels in HNSCC cancer cell lines correlate with migratory and invasive potential.
(A) Quantitative real-time PCR analysis of *LH2* mRNA levels in immortalized oral keratinocytes and HNSCC cell lines. *LH2* expression was normalized to *RPL23* mRNA levels and fold expression was calculated relative to the normal oral keratinocytes; OKF6-TERT cells. Data are presented as the mean ± SEM ($n = 3$ biologic replicates; One-way ANOVA test, $^{*}P < 0.05$, $^{****}P < 0.0001$).
(B) *Left*, western blot showing LH2 protein expression levels in OKF6-TERT oral keratinocytes compared to UM-SCC-5 and UM-SCC-74A cells. This blot is representative of independent biologic replicates. *Right*, quantification of LH2 protein levels. Band intensities were normalized to β-actin and are shown as the fold change relative to LH2 expression in OKF6-TERT oral keratinocytes.
(C) Wound healing (scratch) assay performed with LH2-high UM-SCC-74A versus LH2-low UM-SCC-5 cells. Images were captured every hour for 24 h to quantify rates of wound closure. Data are presented as the mean ± SEM ($n = 3$ biological replicates, with 3 independent FOV per replicate).
(D) Transwell invasion assays were performed for LH2-high UM-SCC-74A versus LH2-low UM-SCC-5 cells using Boyden chambers precoated with Matrigel. After 24 h, cells were stained with 0.05% crystal violet and DAPI, imaged, and counted to quantify rates of invasion. Representative data of independent biologic replicates are presented as the mean ± SD (>5 independent FOV were quantified per biologic replicate).
(E) *Left*, *in vivo* bioluminescent imaging (BLI) of LumiFluor-labeled LH2-high UM-SCC-74A versus LH2-low UM-SCC-5 cells 21 d postorthotopic tongue transplantation. *Right*, BLI signals were quantified by region of interest (ROI) analysis of images obtained at endpoint. Also see Supplementary Figure S1 for ROI definition.

h to stain the collagen fibers. Slides were washed with 0.01 N hydrochloric acid, dehydrated in 100% ethanol and xylene and mounted in resinous medium (DPX Mounting Medium, Electron Microscopy Sciences, cat# 13510). Collagen fibers were observed under polarized light microscopy. Immunohistochemistry was performed as previously described [6].

Statistical analysis

Statistical analyses were performed with GraphPad Prism (version 9) using student's *t*-test, one-way ANOVA or 2-way ANOVA as applicable. Data are presented as mean ± SD or mean ± SEM as indicated in the figure legends.

Results

Elevated LH2 correlates with enhanced HNSCC cell motility and metastasis

LH2 is amplified and transcriptionally upregulated in late-stage human primary HNSCCs and this elevated expression significantly correlates with regional lymph node metastasis (RLNM) and poor patient outcome [48]. To determine if *LH2* levels are associated with invasion and metastasis *in vivo*, *LH2* expression in ten independent cell lines derived from oral and oropharyngeal sites of different patients, representative of both HPV(-) and HPV(+) subtypes, (**Table S1**) was compared to 3 independent normal control oral cell lines (nontransformed, immortalized oral keratinocytes). We found that *LH2* levels across a majority of HNSCC cell lines were overall comparable to oral keratinocytes (**Fig. 1A**). However, UM-SCC-5 cells were found to have significantly lower expression (~5-fold decrease, $P < 0.05$) while SCC-15 and UM-SCC-74A cells displayed significantly higher mRNA expression (~8-fold increase, $P < 0.0001$) relative to oral keratinocytes, a finding also consistent at the protein level in the UM-SCC-74A cells (**Fig. 1A-B**). Notably, isoform-specific analysis of *LH2* expression revealed that both UM-SCC-5 and UM-SCC-74A cells primarily express the LH2b (long) isoform (**Figure S1C**). In contrast to *LH2*, the closely related *LH1* and *LH3* family members displayed near-equivalent levels of expression between the UM-SCC-5 and UM-SCC-74A cells, and the expression of 2 additional collagen-modifying enzymes responsible for

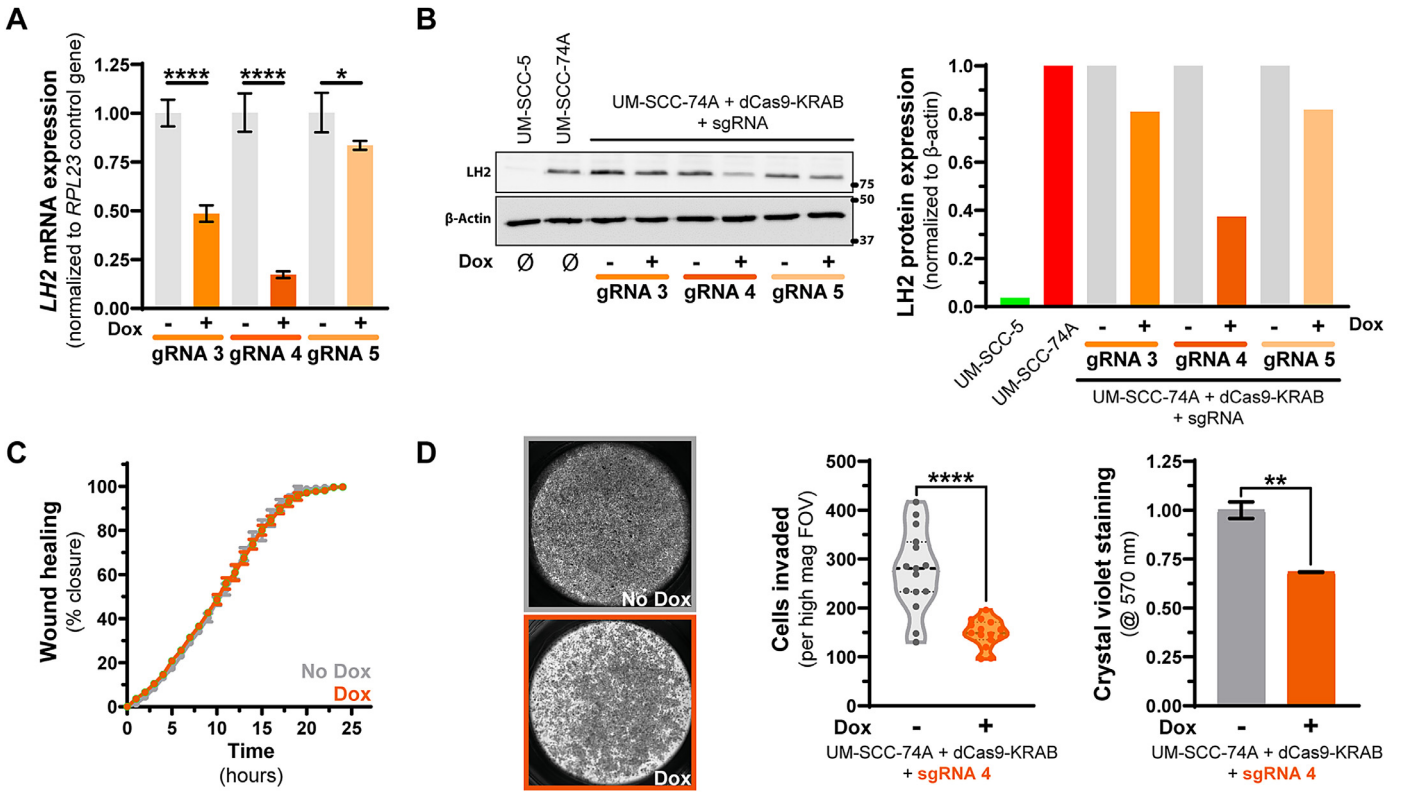

Fig. 2. Repressing *LH2* expression blunts HNSCC cell migration and invasion.
(A) Evaluation of the CRISPRi system for inducible silencing of *LH2* expression. To validate 5 sgRNAs targeting the *PLOD2* gene promoter region, LH2-high UM-SCC-74A cells stably expressing doxycycline-inducible dCas9-KRAB were transduced with each sgRNA, cells were treated +/- 1 μg/mL doxycycline for 7 d, and quantitative real-time PCR was used to assess *LH2* mRNA levels. Representative data of independent biologic replicates are presented as the mean ± SD (4 technical replicates per biologic replicate; Student's *t* test, $^{*}P < 0.05$, $^{****}P < 0.0001$). Also see Supplementary Figure 2A.
(B) *Left*, UM-SCC-74A_TRE3G$^{dCas9\text{-}KRAB}$U6^{sgRNA} cells were treated +/- 1 μg/mL doxycycline for 7 d, total protein extracted, and western blot run to validate repression at the protein level. This blot is representative of independent biological replicates. *Right*, quantification of LH2 protein levels. Band intensities were normalized to *β*-actin and are shown as the fold change relative to the no doxycycline condition.
(C) Wound healing (scratch) assay performed with the stable UM-SCC-74A_TRE3G$^{dCas9\text{-}KRAB}$U6^{sgRNA4} cells treated +/- 1 μg/mL doxycycline for 7 d. Images were captured every hour for 24 h to quantify rates of wound closure. Representative data of independent biologic replicates are presented as the mean ± SD (3 independent FOV were captured and quantified per biologic replicate). Also see Supplementary Figure 2B.
(D) *Left*, transwell invasion assays were performed for UM-SCC-74A_TRE3G$^{dCas9\text{-}KRAB}$U6^{sgRNA4} cells using Boyden chambers precoated with Matrigel. After 24 h, cells were stained with 0.05% crystal violet, imaged, and cell invasion quantified. *Right*, quantification of invasion presented as either the number of cells invaded per field of view (FOV), or by extracting the crystal violet and analyzing absorbance at 570 nm. Representative data of independent biologic replicates are presented as the mean ± SD (>5 independent FOV were quantified per biologic replicate).

initiating collagen cross-linking, *LOX* and *LOXL2*, were also significantly increased (>10-fold, $P < 0.001$) but only in the UM-SCC-11A and UM-SCC-74A cells (**Figure S1A-B**). Since elevated *LH2* has been correlated with aggressive tumor behavior, we next examined the association between expression levels and cell behavior *in vitro* and *in vivo*. Analysis of 2D cell migration in wound healing assays confirmed that the higher *LH2* expression characteristic of UM-SCC-74A cells correlated with enhanced rates of wound closure (~75% increase) compared to UM-SCC-5 cells (**Fig. 1C**). Moreover, higher *LH2* levels also correlated with a dramatic increase in 3D cell invasion through Matrigel in transwell assays for UM-SCC-74A cells compared to UM-SCC-5 cells (**Fig. 1D**). We next investigated the ability of these cell lines to metastasize to regional lymph nodes using a previously established orthotopic tongue transplant model of HNSCC [23, 36, 40]. Quantitative bioluminescent imaging (BLI) of each cell line stably expressing our LumiFluor GpNLuc optical reporter [49] revealed that UM-SCC-74A cells rapidly and consistently develop RLNMs compared to UM-SCC-5 cells *in vivo* (**Fig. 1E** and **S1D**).

LH2 *is necessary for HNSCC invasion and metastatic dissemination*

To directly test the functional role of LH2 toward driving tumor cell migration, invasion and HNSCC disease dissemination, we next performed loss- and gain-of-function studies using the LH2-high (UMSCC-74A) and LH2-low (UMSCC-5) cell lines identified above, respectively. We engineered UM-SCC-74A cells (UM-SCC-74A_TRE3G$^{dCas9\text{-}KRAB}$U6^{sgRNA}) with an inducible CRISPRi repression system (dCas9-KRAB) [17] which allows for the controlled downregulation of *LH2* gene expression (**Figure S2A**). A panel of sgRNAs targeting the *LH2* promoter were designed and validated for efficiency of *LH2* repression at both the RNA and protein levels in stably transduced cell lines. In particular, sgRNA4 produced the most robust decrease (~80% and 60% decrease, respectively) in LH2 levels (**Fig. 2A-B**). Upon Dox-mediated CRISPRi repression, the UM-SCC-74 sgRNA4 stable cells displayed a significant decrease in invasive ability ($P < 0.0001$), however 2D cell migration was not affected by suppressing *LH2* (**Figs. 2C-D** and **S2B**). Beyond its role in collagen-I modification, LH2 has also been shown to

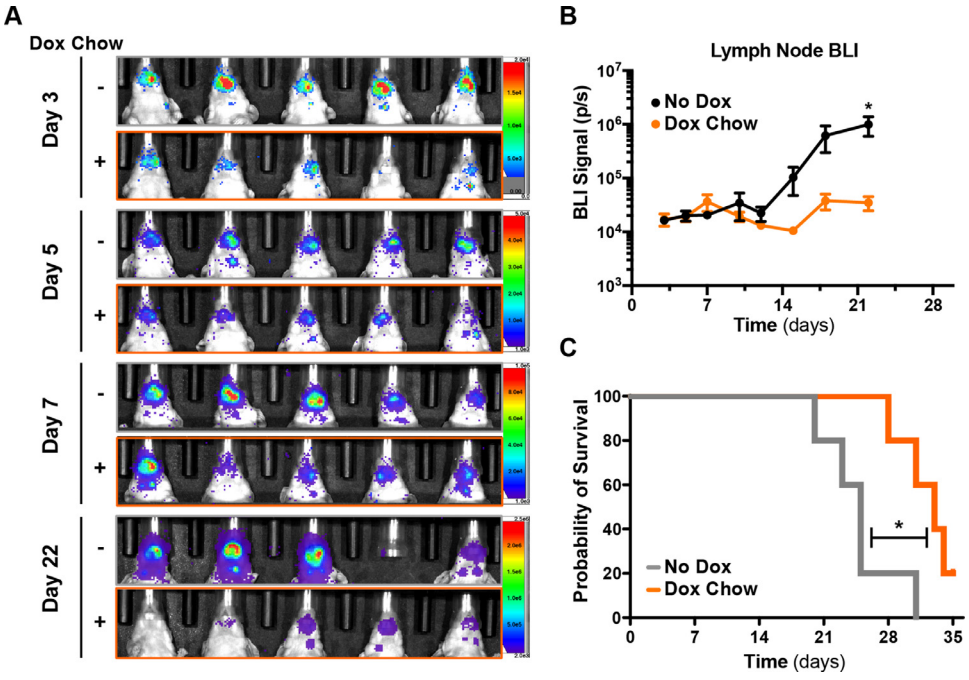

Fig. 3. Repressing *LH2* expression inhibits metastasis and improves overall survival.
(A) Representative *in vivo* BLI images of LumiFluor-labeled UM-SCC-74A_TRE3G$^{dCas9\text{-}KRAB}$U6^{sgRNA4} cells at various times postorthotopic tongue xenograft transplantation in animals administered either normal or doxycycline chow.
(B) Longitudinal quantification of metastatic lymph node BLI signals by ROI analysis of images obtained at various times. Detection of regional lymph node metastases was significantly reduced ($P < 0.05$) in LH2 knockdown mice fed doxycycline compared to control chow animals. Also see Supplementary Figure S1 for ROI definition.
(C) Kaplan-Meier analysis of animals administered either normal or doxycycline chow and monitored at various times postorthotopic tongue transplantation with UM-SCC-74A_TRE3G$^{dCas9\text{-}KRAB}$U6^{sgRNA4} cells. Tumor progression was significantly reduced ($P < 0.05$) in LH2 knockdown mice fed doxycycline (median overall survival = 32 d) compared to control chow animals (median overall survival = 25 d).

play a critical role in integrin-β1 activation in HNSCC cells [57], which may explain why LH2 knockdown robustly retards tumor cell invasion but does not significantly affect 2D cell migration. Based on these findings, we next examined whether repressing LH2 levels affects the efficiency of metastasis *in vivo* using the orthotopic tongue transplant model. Orthotopic xenografts were established with UM-SCC-74A_TRE3G$^{dCas9\text{-}KRAB}$U6^{sgRNA} cells and mice were maintained on either normal or Dox chow to induce CRISPRi-mediated repression of *LH2*. Knockdown of LH2 *in vivo* led to a significant reduction in RLNM burden compared to the control group. (**Figs. 3A-B**). Moreover, *LH2* downregulation significantly prolonged disease-specific overall survival ($P < 0.05$) and decreased the onset of tumor-induced weight loss, which could be driven in part by a slight reduction in overall tumor volumes at endpoint (**Fig. 3C** and **S3A-B**).

LH2 *overexpression is sufficient to enhance HNSCC cell migration, invasion and promote metastasis* in vivo

Our loss-of-function findings indicated that LH2 is necessary for promoting aggressive, invasive cell behavior *in vitro* and metastasis *in vivo*. Next, to determine if *LH2* expression is sufficient to regulate these processes, we engineered gain-of-function UM-SCC-5 cells (UM-SCC-5_PGK^{TetOn3G}TRE3G^{LH2}) with an inducible Tet-on 3G system (TRE3G; rtTA^3) which enables precise, reversible, and efficient inducible control of ectopic *LH2* gene expression (**Figure S4A**). Dox dose-titration experiments with this cell line demonstrated robust >500-fold induction of LH2 at both the RNA and protein levels in stably transduced cell lines using as little as 125 ng/mL Dox (**Fig. 4A-B**). Notably, the induced LH2 protein levels were comparable to levels observed in the highly metastatic UMSCC-74A cell line. LH2 overexpression led to significantly faster wound closure (~2x faster, $P < 0.001$) and a significant increase ($P < 0.0001$) in 3D invasion in the dox-induced UM-SCC-5_PGK^{TetOn3G}TRE3G^{LH2} cells compared to control (**Fig. 4C-D** and **S4B**). Consequently, orthotopic xenografts established with these cells gave rise to robust RLNM (cervical lymph nodes) by 21 d post-transplant in animals administered Dox chow compared to animals maintained on a control diet (**Fig. 5A**). Remarkably, e*x vivo* BLI of surgically resected tissues confirmed the presence of local metastases to the cervical lymph nodes as well as distant metastases to the liver (**Fig. 5B-C** and **S5B**). Additionally, pan-cytokeratin staining confirmed the presence of lymph node metastasis only in the LH2-overexpressing SCC-5 tumors (**Fig. 5C, *right***) Importantly, analysis of intraoral tumor volumes throughout the experiment and tumor volumes at endpoint demonstrate that *LH2* overexpression does not affect primary tumor growth rate or size (**Fig. 5D** and **S5C**). Collectively, these data indicate that, while LH2 does not appear to play a major role in driving primary tumor growth and survival, its expression is necessary and sufficient to augment tumor cell invasive behaviors and promote metastatic dissemination *in vivo*.

LH2 upregulation changes collagen cross-link quality in the tumor ECM without affecting overall cross-link quantity

As described above, collagen cross-linking is initiated by the formation of Lys^{ald} or Hyl^{ald} in collagen telopeptides via the action of LOX and LOXL1–4 (**Figure S6**). Depending on the state of Lys hydroxylation in collagen telopeptides, 2 major cross-linking pathways are evolved: Lys^{ald}- and Hyl^{ald}-

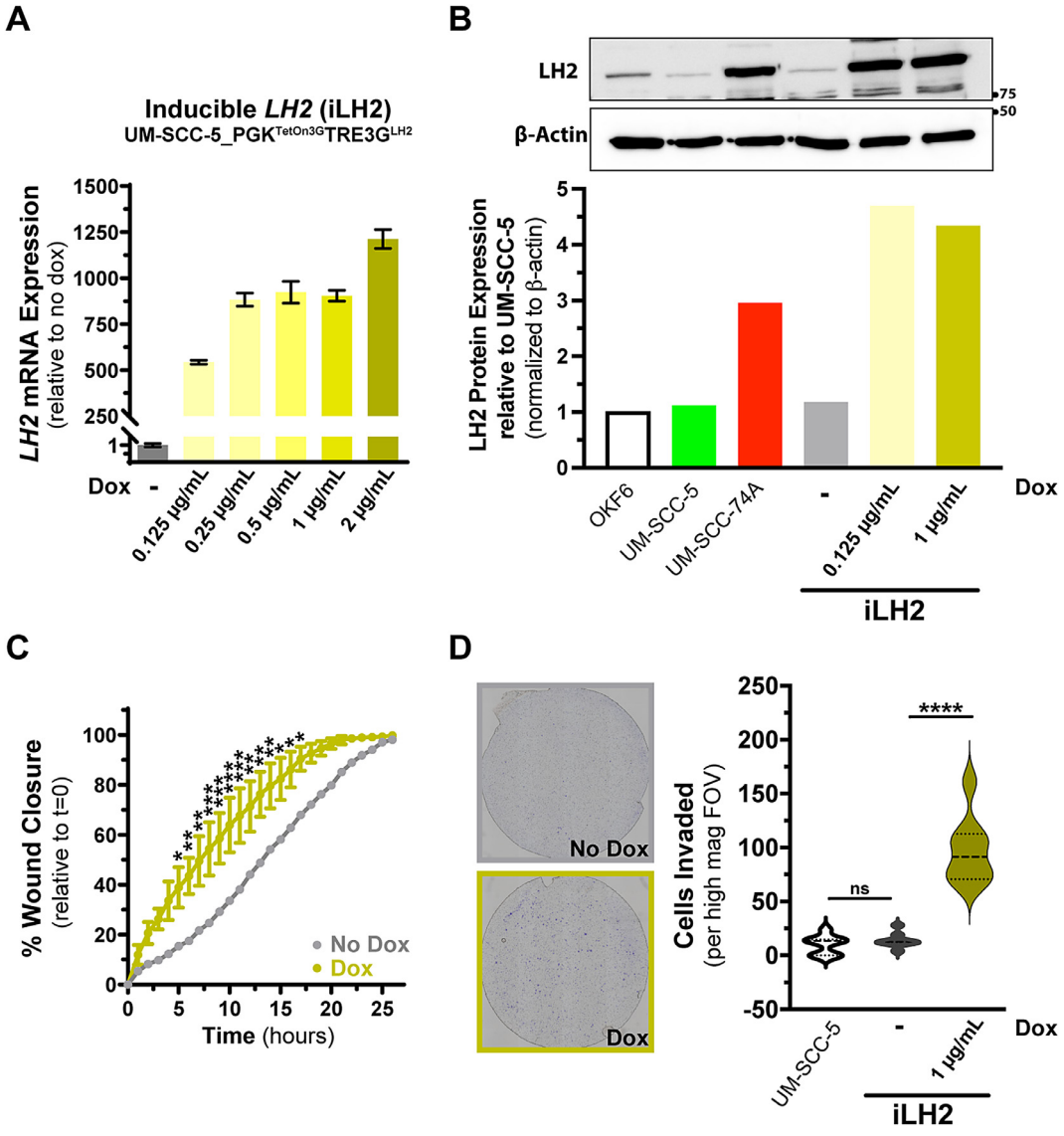

Fig. 4. Ectopic *LH2* overexpression in *LH2*-low cells augments HNSCC migration and invasion.
(A) Evaluation of the doxycycline inducible Tet-On 3G system for inducing *LH2* expression. Quantitative real-time PCR analysis of *LH2* mRNA levels in UM-SCC-5_PGK^{TetOn3G}TRE3G^{LH2} cells treated with increasing concentrations of doxycycline for 72 hrs. Representative data of independent biologic replicates are presented as the mean ± SD (4 technical replicates per biologic replicate).
(B) *Top*, UM-SCC-5_PGK^{TetOn3G}TRE3G^{LH2} cells were treated with the indicated concentrations of doxycycline for 72 h, total protein extracted, and western blot run to validate induced expression at the protein level. This blot is representative of independent biologic replicates. *Bottom*, quantification of LH2 protein levels. Band intensities were normalized to β-actin and are shown as the fold change relative to the no doxycycline condition.
(C) Wound healing (scratch) assay performed with UM-SCC-5_PGK^{TetOn3G}TRE3G^{LH2} cells treated +/- 1 µg/mL doxycycline for 72 h. Images were captured every hour for 24 h to quantify rates of wound closure. Representative data of independent biologic replicates are presented as the mean ± SD (3 independent FOV were captured and quantified per biologic replicate; Two-way ANOVA test with Sidak correction, $^{*}P < 0.05$, $^{**}P < 0.01$, $^{***}P < 0.001$).
(D) Transwell invasion assays were performed for UM-SCC-5_PGK^{TetOn3G}TRE3G^{LH2} cells treated +/- doxycycline using Boyden chambers precoated with Matrigel. Cells were stained with 0.05% crystal violet after 24 h, imaged, and cell invasion quantified. Representative data of independent biologic replicates are presented as the mean ± SD (>5 independent FOV was quantified per biologic replicate; Student's *t* test, ns = not significant, $^{****}P < 0.0001$).

derived cross-links [63], with the latter displaying enhanced stability over the former. Since LH2 is responsible for Lys hydroxylation in telopeptides, its activity is key to determining the stability, that is, "quality", of collagen cross-linking [8, 20, 61]. While LH2 hyperactivity has been implicated in fibrosis for decades [59, 60], mounting evidence suggests that LH2 upregulation can also drive proinvasive and prometastatic tumor behaviors across many different cancers.

To characterize the effect of *LH2* levels on the collagen cross-link profiles in our orthotopic HNSCC model, we analyzed primary tumors isolated from UM-SCC-5_PGK^{TetOn3G}TRE3G^{LH2}-transplanted tongues of animals administered either normal or Dox chow and performed histology and immunohistochemistry (**Fig. 6A**). Analysis of Picrosirius red staining under polarized light revealed that the amount of fibrillar collagens in animals administered Dox chow was significantly higher and more mature

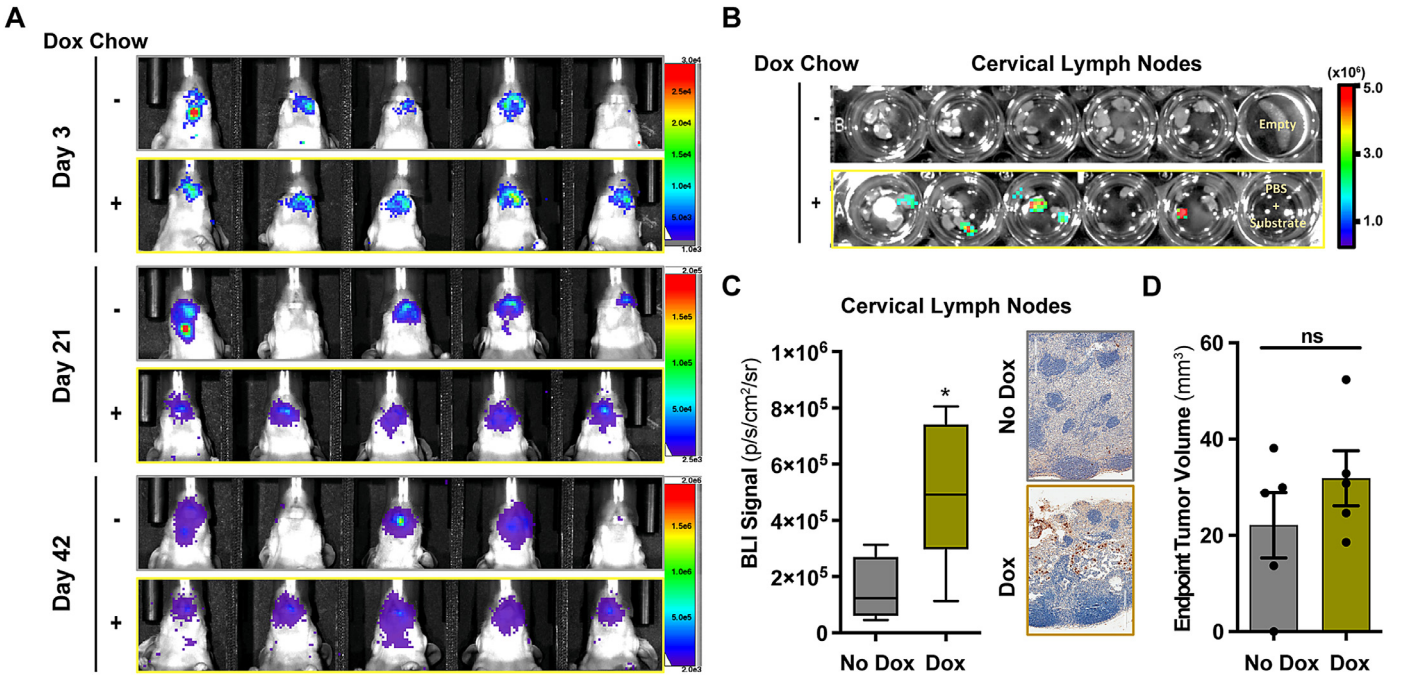

Fig. 5. Increased *LH2* expression is sufficient to drive HNSCC tumor metastasis.
(A) Representative *in vivo* BLI images of LumiFluor-labeled UM-SCC-5_PGK^{TetOn3G}TRE3G^{LH2} cells at various times postorthotopic tongue transplantation in animals administered either normal or doxycycline chow.
(B) Representative *ex vivo* BLI images of cervical lymph nodes resected from control- and doxycycline-chow fed animals at study endpoint.
(C) Quantification of metastatic lymph node *ex vivo* BLI signals by ROI analysis of images obtained at endpoint. Detection of regional lymph node metastases was significantly increased in induced *LH2* overexpression mice fed doxycycline compared to control chow animals. ($n = 5$ mice per group, mean ± SEM; Student's t test, $P < 0.05$).
(D) Primary orthotopic tumor volumes are similar in control- and doxycycline-chow fed animals at study endpoint. ($n = 5$ mice per group, mean ± SEM; Student's t test, ns = not significant).

as indicated by orange-bright red color compared to control (No Dox) diet animals (greenish yellow-orange) or nontransplanted normal tongues. Amino acid analysis revealed that collagen composition (collagen/total proteins) was identical (20–25%) across the normal, No Dox and Dox groups (**Fig. 6B**). The Hyl level per collagen was slightly but significantly higher in the No Dox group when compared to normal, which could be due to slight differences in tissue sampling (i.e., geographic location of the tumor tissue piece that was processed for analysis). Importantly, though, there was no difference between the normal and Dox, or the No Dox and Dox groups. However, quantitative collagen cross-link analysis revealed that the tumor tissue in the *LH2* overexpression group contained high LH2-mediated Hyl^{ald}-derived collagen cross-links (HLCCs) compared to control animals (**Fig. 6C**). Furthermore, the ratio of HLCC (DHLNL and HLNL cross-links) to Lys^{ald}-derived collagen cross-links (LCCs, HHMD) was significantly increased with *LH2* overexpression. HLNL was not included in the ratio since it can be derived from Lys^{ald}- or Hyl^{ald} [63]. However, considering that LH2 levels are high in tumor tissues (i.e., telopeptidyl Lys hydroxylation), a significant amount of the HLNL in tumors is likely derived from the Hyl^{ald}. In this case, the ratio of HLCCs to LCC in tumors is expected to be even higher. Collectively, these findings confirm that the stable collagen cross-links mediated by increased LH2 activity are responsible for generating a modified tumor ECM that promotes tumor metastasis.

Discussion

Invasive tumor phenotypes are responsible for the poor overall survival observed in patients with advanced HNSCC. These aggressive, metastatic cases are often associated with a desmoplastic ECM characterized by excessive accumulation of fibrillar collagens [44, 62]. Utilizing a well-established orthotopic HNSCC model, we identified a functional role for LH2-mediated collagen modification in tumor progression to metastasis. Our findings corroborate previous studies indicating a role for collagen cross-linking in HNSCC disease severity [48] and mechanistically elaborate upon previous reports suggesting that LH2-mediated HLCC collagen cross-links are associated with metastatic dissemination. A recent report from Ueki and colleagues [57] found that elevated LH2 expression activates Integrin β-1 driven cell migration, invasiveness and tumor dissemination of HNSCC tumors, further implicating LH2 in regulating HNSCC metastasis and disease outcome. Thus, LH2 levels may have prognostic value in predicting disease progression, while also serving as an actionable therapeutic target for prophylactic treatments aimed at preventing HNSCC tumor progression and adverse disease outcomes.

Accumulating evidence indicates that increased lysyl hydroxylase (LH) activity derived from both tumor intrinsic and extrinsic sources (e.g. cancer associated fibroblasts) is associated with tumor progression in many cancers [9, 38, 62]. While all LHs appear to be able to hydroxylate Lys residues in the helical domain of collagen, only LH2 is capable of catalyzing hydroxylation of telopeptidyl Lys residues, a prerequisite to form Hyl^{ald}-derived stable collagen cross-links. Thus, there is significant interest in therapeutic strategies capable of inhibiting LH2 activity and blunting tumor progression. Notably, LH2 is part of a superfamily of oxygenases that require **α**-ketoglutarate (**α**KG) for their enzymatic activity. A recent high-throughput small molecule drug screen identified KD-1 (4,4,4-Trifluoro-1-(pyridine-3-yl)-1,3-butanedione) using a novel luminescence-based assay that measures LH2 activity based on

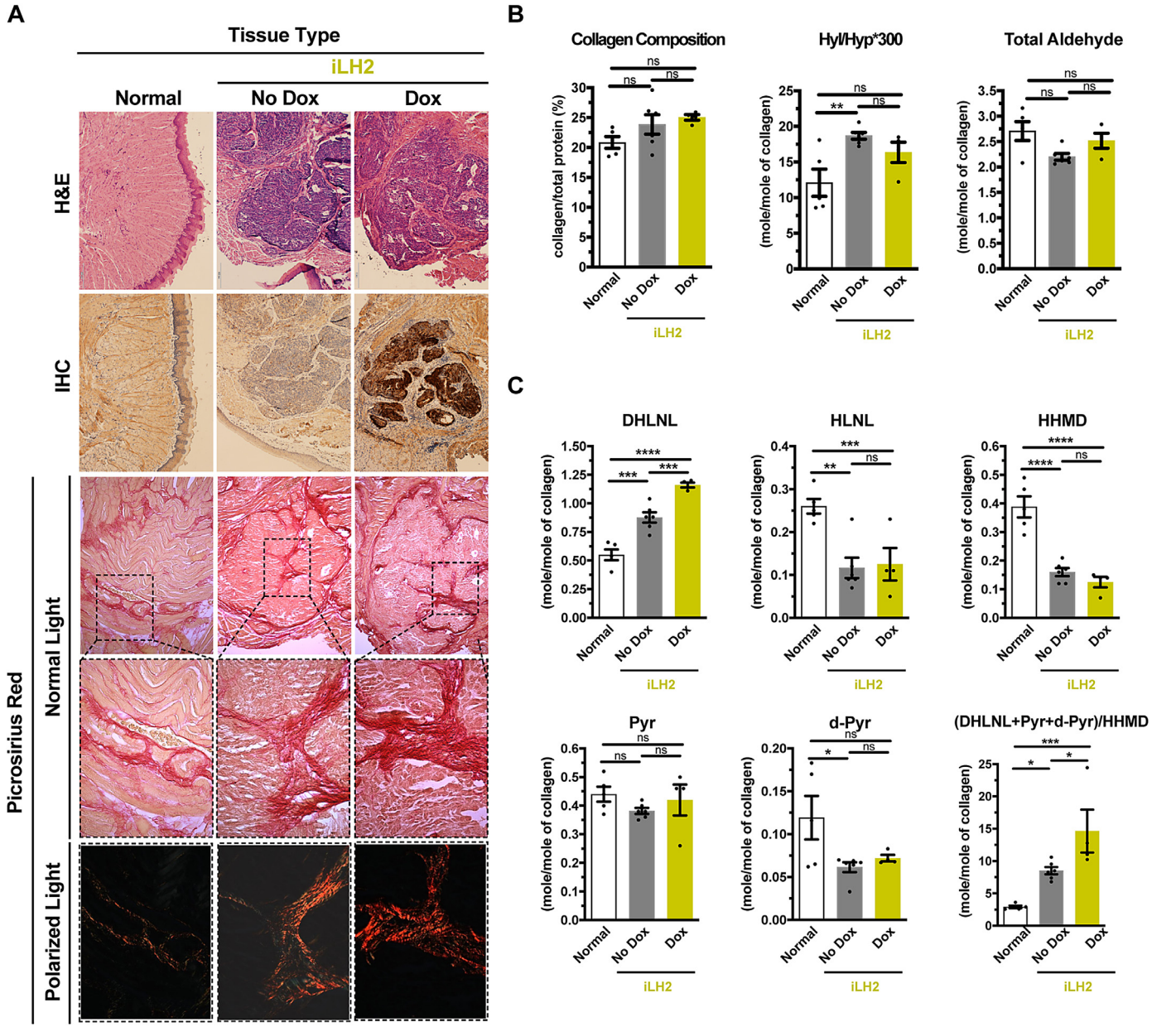

Fig. 6. LH2 upregulation in HNSCC cells remodels collagen cross-link quality but not total cross-link quantity in the tumor microenvironment.
(A) Histologic and immunohistochemical analysis of LH2 levels and LH2-induced fibrillar collagen tracks. Representative coronal sections from resected tongues of animals transplanted with UM-SCC-5_PGK^{TetOn3G}TRE3G^{LH2} cells and administered either normal or doxycycline chow. Tissues were formalin fixed, embedded, and stained images of normal tongue versus SCC5 +/- LH2 overexpression primary tumors were captured for H&E, IHC staining for LH2, and Picrosirius Red staining for collagen fibrils.
(B) Total collagen cross-link quantities in naïve normal tissues were compared to animals transplanted with UM-SCC-5_PGK^{TetOn3G}TRE3G^{LH2} cells and administered either normal or doxycycline chow. Quantification of total collagen cross-links, aldehyde levels, and the ratio of hydroxylysine (Hyl) to hydroxyproline content (Hyp/Hyp x 300). Data are presented as the mean ± SEM ($n = 4$-6 mice per group; One-way ANOVA with Fischer's LSD test, ns = not significant, $^{**}P < 0.01$).
(C) Analysis of collagen cross-link quality in naïve normal tissues were compared to animals transplanted with UM-SCC-5_PGK^{TetOn3G}TRE3G ^{LH2} cells and administered either normal or doxycycline chow. Quantification of DHLNL, HLNL, HHMD, Pyr, d-Pyr and the ratios of DHLNL-to-HLNL, Pyr-to-dPyr, or HLCC-to-LCC [(DHLNL+Pyr+d-Pyr)/HHMD] were calculated. Data are presented as the mean ± SEM ($n = 4$-6 mice per group; One-way ANOVA with Fischer's LSD test, ns = not significant, $^{*}P < 0.05$, $^{**}P < 0.01$, $^{***}P < 0.001$, $^{****}P < 0.0001$).

the amount of succinate produced from **α**KG. Since **α**KG is a rate-limiting metabolic intermediate of the TCA cycle, these results suggest that treatment of LH2-high tumors with KD-1 may lead to an accumulation of intratumoral **α**KG levels [12, 22]. Interestingly, recent work has demonstrated that reduced **α**KG levels are associated with the premalignant to malignant transition and interventions that lead to elevated **α**KG promote tumor cell differentiation and halt tumor progression [34]. Therefore, our findings have clear translational implications since strategies to inhibit LH2 may not only disrupt collagen cross-linking and tumor metastasis but may also lead to increased **α**KG levels that promote tumor cell differentiation and a less aggressive phenotype. Future studies aimed at investigating these exciting possibilities are warranted.

The TME is largely composed of ECM, whose composition, biochemical, and biophysical properties are known to influence the differentiation, proliferation, survival, migration, and invasion of tumor cells [25]. Fibrillar collagens such as types I and III, especially type I collagen [55], are the major constituents of solid tumor ECM. These collagens provide stability and tensile strength to tissues and therefore contribute to the stiffness observed in desmoplastic cancers such as HNSCCs. The tensile strength of collagen fibrils is achieved by formation of covalent intermolecular cross-linking initiated by LOX/LOXL1-4 [56]. However, the stability of collagen fibrils also depends on the quality/type of cross-links formed, not necessarily the quantity of cross-links alone. Collagens containing LH2-mediated stable cross-links are more resistant to degradation than those not modified by LH2 [8, 20, 61]. Moreover, such a stiffened and highly cross-linked tumor ECM may diminish accessibility of immune cells to the cancer cells within the TME. Immune exclusion from tumors can occur by several mechanisms including suppression of antigen processing machinery, impaired immune cell trafficking, impaired infiltration into tumors, poor T cell activation, and/or establishment of a PD-1/PD-L1 checkpoint [2, 3, 7]. Notably, tumor-associated hypoxia induces TGF-β1, which not only promotes exclusion of T lymphocytes from tumors [31, 43, 54] but also functions as a key driver of *LH2* and *LOX/LOXL2* gene expression [15, 47], thus creating a direct association between tumor hypoxia, ECM stiffness, mechano-sensation [57], and immunosuppression [41].

Conclusions

The present study sheds new insight into the role that the tumor ECM – established by LH2-mediated cross-links – plays in promoting HNSCC metastasis. Several studies have suggested that increased total collagen cross-links resulting from upregulation of LOX family members are associated with poor prognosis in patients with breast, lung, and oral cancers [28, 42, 48, 50]. However, here we show that knockdown of LH2 alone is sufficient to blunt invasion and metastasis despite robust cellular expression of LOX and LOXL2. This indicates that the quality/type of collagen cross-links (i.e. stability), and not simply the total quantity of cross-links, is a necessary and crucial driver of HNSCC metastatic dissemination. Lastly, a limitation of our study is the number of HNSCC cell line models tested. However, given the striking nature of our findings and their potential disease relevance toward HNSCC patient outcomes, it is both prudent and urgent that these studies be further validated in additional independent HNSCC model systems.

Author contributions

Conception and design: K.P-S., M.Y., and A.L.A.

Development of methodology: K.S., K.P-S., M.T., and A.L.A.

Acquisition of data (provided animals, acquired and managed patients, provided facilities, etc.): K.S., K.P-S., A.M.M., M.T., and R.M.M.

Interpretation of data (e.g., statistical analysis, biostatistics, computational analysis): K.S., K.P-S., M.T., M.Y. and A.L.A.

Writing of the manuscript: K.S., K.P-S, M.Y., and A.L.A.

Review and revision of the manuscript: K.S., K.P-S., A.M.M., M.T., M.Y., and A.L.A.

Administrative, technical, or material support (i.e., reporting or organizing data, constructing databases): M.R.R., H.H., M.Y., and A.L.A.

Study supervision: M.Y. and A.L.A.

Acquisition of funding: A.L.A.

Declaration of competing interest

The authors declare no competing interests.

Funding

This work was supported by a NIH/NIDCR F31-DE028749 training grant (to R.M. Murphy), University Cancer Research Fund (UCRF; to A.L. Amelio), a UNC Lineberger Tier 3 Developmental Award (to A.L. Amelio), and in part by a Developmental Research Program Grant from the Yale Head and Neck SPORE NIDCR P50-DE030707 (to A.L. Amelio). The UNC Lineberger Small Animal Imaging, Flow Cytometry, and Translational Pathology Lab are supported in part by the NCI Center Core Support Grant P30-CA016086 to the UNC Lineberger Comprehensive Cancer Center. The UNC Flow Cytometry Core Facility is also supported by the North Carolina Biotech (NCBT) Center Institutional Support Grant 2012-IDG-1006. The Translational Pathology Lab is also supported by NIH U54-CA156733, NIEHS P30-EOS010126, and NCBT 2015-IDG-1007.

Acknowledgments

The authors thank Wendell Yarbrough, Barbara Savoldo, Gianpietro Dotti, and members of the Amelio Lab for helpful discussions, suggestions, and/ or scientific review of this manuscript. We thank Drs. Johannes Zuber for kindly providing the pRRL-rtTA3 lentiviral vector, Jim Rheinwald for kindly providing the normal immortalized OKF4-TERT and OKF6-TERT keratinocyte cell lines, Valerie Murrah for kindly providing the normal immortalized GMSM-K keratinocyte cell line, Thomas Carey for kindly providing the UM-SCC-5, UM-SCC-11A, UM-SCC-14A, UM-SCC-74A, UM-SCC-15, and UM-SCC-25 HNSCC cell lines, and Randall Kimple for kindly providing the UM-SCC-47, UM-SCC-2, SCC-090 and 93-VU-147T cell lines.

Supplementary materials

Supplementary material associated with this article can be found, in the online version, at doi:10.1016/j.neo.2021.05.014.

References

[1] Barker HE, Cox TR, Erler JT. The rationale for targeting the LOX family in cancer. *Nature Reviews Cancer* 2012;**12**:540–52.

[2] Binnewies M, Roberts EW, Kersten K, Chan V, Fearon DF, Merad M, Coussens LM, Gabrilovich DI, Ostrand-Rosenberg S, Hedrick CC. Understanding the tumor immune microenvironment (TIME) for effective therapy. *Nat Med*. (Nature Publishing Group); 2018. p. 541–50.

[3] Bonaventura P, Shekarian T, Alcazer V, Valladeau-Guilemond J, Valsesia-Wittmann S, Amigorena S, Caux C, Depil S. Cold tumors: a therapeutic challenge for immunotherapy. *Front. Immunol.* 2019;**10**:168.

[4] Bray F, Ferlay J, Soerjomataram I, Siegel RL, Torre LA, Jemal A. Global cancer statistics 2018: GLOBOCAN estimates of incidence and mortality worldwide for 36 cancers in 185 countries. *CA Cancer J. Clin.* 2018;**68**:394–424.

[5] Brenner JC, Graham MP, Kumar B, Saunders LM, Kupfer R, Lyons RH, Bradford CR, Carey TE. Genotyping of 73 UM-SCC head and neck squamous cell carcinoma cell lines. *Head neck* 2010;**32**:417–26.

[6] Carper MB, Troutman S, Wagner BL, Byrd KM, Selitsky SR, Parag-Sharma K, Henry EC, Li W, Parker JS, Montgomery SA. An immunocompetent mouse model of HPV16(+) head and neck squamous cell carcinoma. *CellReports* 2019;**29**:1660–74 e1667.

[7] Chen IX, Chauhan VP, Posada J, Ng MR, Wu MW, Adstamongkonkul P, Huang P, Lindeman N, Langer R, Jain RK. Blocking CXCR4 alleviates desmoplasia, increases T-lymphocyte infiltration, and improves immunotherapy in metastatic breast cancer. *Proceedings of the National Academy of Sciences of the United States of America* 2019;**116**:4558–66.

[8] Chen Y, Terajima M, Yang Y, Sun L, Ahn Y-H, Pankova D, Puperi DS, Watanabe T, Kim MP, Blackmon SH. Lysyl hydroxylase 2 induces a collagen cross-link switch in tumor stroma. *The Journal of Clinical Investigation* 2015;**125**:1147–62.

[9] Chen Y, Terajima M, Yang Y, Sun L, Ahn Y-H, Pankova D, Puperi DS, Watanabe T, Kim MP, Blackmon SH. Lysyl hydroxylase 2 induces a collagen cross-link switch in tumor stroma. *J. Clin. Invest.* 2015:1147–62 (American Society for Clinical Investigation).

[10] Fitzmaurice C, Allen C, Barber RM, Barregard L, Bhutta ZA, Brenner H, Dicker DJ, Chimed-Orchir O, Dandona R, et al.Collaboration, G.B.o.D.C. Global, regional, and national cancer incidence, mortality, years of life lost, years lived with disability, and disability-adjusted life-years for 32 cancer groups, 1990 to 2015: a systematic analysis for the global burden of disease study. *JAMA Oncol*; 2017. (American Medical Association) p. 524–48.

[11] Cox TR, Gartland A, Erler JT. Lysyl oxidase, a targetable secreted molecule involved in cancer metastasis. *Cancer Res* 2016;**76**:188–92.

[12] Devkota AK, Veloria JR, Guo H-F, Kurie JM, Cho EJ, Dalby KN. Development of a High-Throughput Lysyl Hydroxylase (LH) Assay and Identification of Small-Molecule Inhibitors against LH2. *SLAS discovery: advancing life sciences R & D* 2019;**24**:484–91.

[13] Dickson MA, Hahn WC, Ino Y, Ronfard V, Wu JY, Weinberg RA, Louis DN, Li FP, Rheinwald JG. Human keratinocytes that express hTERT and also bypass a p16(INK4a)-enforced mechanism that limits life span become immortal yet retain normal growth and differentiation characteristics. *In Mol. Cell. Biol.* 2000:1436–47.

[14] Eisinger-Mathason TSK, Zhang M, Qiu Q, Skuli N, Nakazawa MS, Karakasheva T, Mucaj V, Shay JES, Stangenberg L, Sadri N, et al. Hypoxia-dependent modification of collagen networks promotes sarcoma metastasis. *Cancer Discovery* 2013;**3**:1190–205.

[15] Erler JT, Bennewith KL, Nicolau M, Dornhöfer N, Kong C, Le Q-T, Chi J-TA, Jeffrey SS, Giaccia AJ. Lysyl oxidase is essential for hypoxia-induced metastasis. *Nature* 2006;**440**:1222–6.

[16] Filipe EC, Chitty JL, Cox TR. Charting the unexplored extracellular matrix in cancer. *Int. J. Exp. Pathol.* 2018;**99**:58–76.

[17] Fulco CP, Munschauer M, Anyoha R, Munson G, Grossman SR, Perez EM, Kane M, Cleary B, Lander ES, Engreitz JM. Systematic mapping of functional enhancer-promoter connections with CRISPR interference. *Science (New York, NY)* 2016;**354**:769–73.

[18] Gilchrist EP, Moyer MP, Shillitoe EJ, Clare N, Murrah VA. Establishment of a human polyclonal oral epithelial cell line. *Oral Surgery, Oral Medicine, Oral Pathology, Oral Radiology, and Endodontics* 2000;**90**:340–7.

[19] Gilkes DM, Bajpai S, Wong CC, Chaturvedi P, Hubbi ME, Wirtz D, Semenza GL. Procollagen lysyl hydroxylase 2 is essential for hypoxia-induced breast cancer metastasis. *Molecular Cancer Research: MCR* 2013;**11**:456–66.

[20] Gistelinck C, Weis M, Rai J, Schwarze U, Niyazov D, Song KM, Byers PH, Eyre DR. Abnormal bone collagen cross-linking in osteogenesis imperfecta/bruck syndrome caused by compound heterozygous PLOD2 mutations. *JBMR Plus* 2021;**5**:e10454.

[21] Guo H-F, Bota-Rabassedas N, Terajima M, Leticia Rodriguez B, Gibbons DL, Chen Y, Banerjee P, Tsai C-L, Tan X, Liu X. A collagen glucosyltransferase drives lung adenocarcinoma progression in mice. *Communications biology* 2021;**4** 482-410.

[22] Guo H-F, Cho EJ, Devkota AK, Chen Y, Russell W, Phillips GN, Yamauchi M, Dalby KN, Kurie JM. A scalable lysyl hydroxylase 2 expression system and luciferase-based enzymatic activity assay. *Archives of Biochemistry and Biophysics* 2017;**618**:45–51.

[23] Inglehart RC, Scanlon CS, D'Silva NJ. Reviewing and reconsidering invasion assays in head and neck cancer. *Oral Oncol* 2014;**50**:1137–43.

[24] Johnson DE, Burtness B, Leemans CR, Lui VWY, Bauman JE, Grandis JR. Head and neck squamous cell carcinoma. *Nature Reviews Disease Primers* 2020;**6**:1–22.

[25] Kai F, Drain AP, Weaver VM. The Extracellular Matrix Modulates the Metastatic Journey. *Developmental cell* 2019;**49**:332–46.

[26] Kawashiri S, Tanaka A, Noguchi N, Hase T, Nakaya H, Ohara T, Kato K, Yamamoto E. Significance of stromal desmoplasia and myofibroblast appearance at the invasive front in squamous cell carcinoma of the oral cavity. *Head & Neck* 2009;**31**:1346–53.

[27] Le CC, Bennasroune A, Langlois B, Salesse S, Boulagnon-Rombi C, Morjani H, Dedieu S, Appert-Collin A. Functional Interplay Between Collagen Network and Cell Behavior Within Tumor Microenvironment in Colorectal Cancer. *Front. Oncol.* 2020;**10**:527.

[28] Levental KR, Yu H, Kass L, Lakins JN, Egeblad M, Erler JT, Fong SFT, Csiszar K, Giaccia A, Weninger W, et al. Matrix crosslinking forces tumor progression by enhancing integrin signaling. *Cell* 2009;**139**:891–906.

[29] Lo CM, Wang HB, Dembo M, Wang YL. Cell movement is guided by the rigidity of the substrate. *Biophys. J.* 2000;**79**:144–52.

[30] Mandegar MA, Huebsch N, Frolov EB, Shin E, Truong A, Olvera MP, Chan AH, Miyaoka Y, Holmes K, Spencer CI. CRISPR Interference Efficiently Induces Specific and Reversible Gene Silencing in Human iPSCs. *In Cell Stem Cell* 2016:541–53.

[31] Mariathasan S, Turley SJ, Nickles D, Castiglioni A, Yuen K, Wang Y, Kadel EE, Koeppen H, Astarita JL, Cubas R. TGFβ attenuates tumour response to PD-L1 blockade by contributing to exclusion of T cells. *Nature* 2018;**554**:544–8.

[32] Martin A, Salvador F, Moreno-Bueno G, Floristán A, Ruiz-Herguido C, Cuevas EP, Morales S, Santos V, Csiszar K, Dubus P. Lysyl oxidase-like 2 represses Notch1 expression in the skin to promote squamous cell carcinoma progression. *EMBO J* 2015;**34**:1090–109.

[33] Mochida Y, Parisuthiman D, Pornprasertsuk-Damrongsri S, Atsawasuwan P, Sricholpech M, Boskey AL, Yamauchi M. Decorin modulates collagen matrix assembly and mineralization. *Matrix Biology: Journal of the International Society for Matrix Biology* 2009;**28**:44–52.

[34] Morris JP, Yashinskie JJ, Koche R, Chandwani R, Tian S, Chen C-C, Baslan T, Marinkovic ZS, Sánchez-Rivera FJ, Leach SD. α-Ketoglutarate links p53 to cell fate during tumour suppression. *Nature* 2019;**573**:595–9.

[35] Musicant, A.M., Parag-Sharma, K., Gong, W., Sengupta, M., Chatterjee, A., Henry, E.C., Tsai, Y.-H., Hayward, M., Sheth, S., Betancourt, R., et al. (2020). CRTC1-MAML2 Establishes a PGC1α-IGF1 Circuit that Confers Vulnerability to PPARγ Inhibition. bioRxiv, 2020.2006.2003.129668.

[36] Myers JN, Holsinger FC, Jasser SA, Bekele BN, Fidler IJ. An orthotopic nude mouse model of oral tongue squamous cell carcinoma. *Clinical Cancer Research: An Official Journal of the American Association for Cancer Research* 2002;**8**:293–8.

[37] Oudin MJ, Jonas O, Kosciuk T, Broye LC, Guido BC, Wyckoff J, Riquelme D, Lamar JM, Asokan SB, Whittaker C. Tumor Cell-Driven Extracellular Matrix Remodeling Drives Haptotaxis during Metastatic Progression. *Cancer Discov.* (American Association for Cancer Research); 2016. p. 516–31.

[38] Pankova D, Chen Y, Terajima M, Schliekelman MJ, Baird BN, Fahrenholtz M, Sun L, Gill BJ, Vadakkan TJ, Kim MP. Cancer-Associated Fibroblasts Induce a Collagen Cross-link Switch in Tumor Stroma. *Molecular Cancer Research: MCR* 2016;**14**:287–95.

[39] Paszek MJ, Zahir N, Johnson KR, Lakins JN, Rozenberg GI, Gefen A, Reinhart-King CA, Margulies SS, Dembo M, Boettiger D. Tensional homeostasis and the malignant phenotype. *Cancer Cell* 2005;**8**:241–54.

[40] Patel V, Marsh CA, Dorsam RT, Mikelis CM, Masedunskas A, Amornphimoltham P, Nathan C-AO, Nathan CA, Singh B, Weigert R. Decreased lymphangiogenesis and lymph node metastasis by mTOR inhibition in head and neck cancer. *Cancer Res* 2011;**71**:7103–12.

[41] Peng DH, Rodriguez BL, Diao L, Chen L, Wang J, Byers LA, Wei Y, Chapman HA, Yamauchi M, Behrens C. Collagen promotes anti-PD-1/PD-L1 resistance in cancer through LAIR1-dependent CD8+ T cell exhaustion. *Nature Communications* 2020;**11** 4520-4518.

[42] Peng DH, Ungewiss C, Tong P, Byers LA, Wang J, Canales JR, Villalobos PA,

Uraoka N, Mino B, Behrens C. ZEB1 induces LOXL2-mediated collagen stabilization and deposition in the extracellular matrix to drive lung cancer invasion and metastasis. *Oncogene* 2017;**36**:1925–38.

[43] Peranzoni E, Rivas-Caicedo A, Bougherara H, Salmon H, Donnadieu E. Positive and negative influence of the matrix architecture on antitumor immune surveillance. *Cellular and Molecular Life Sciences* 2013;**70**:4431–48.

[44] Piersma B, Hayward MK, Weaver VM. Fibrosis and cancer: A strained relationship. Biochimica et biophysica acta. *Reviews on Cancer* 2020;**1873**:188356.

[45] Pornprasertsuk S, Duarte WR, Mochida Y, Yamauchi M. Lysyl hydroxylase-2b directs collagen cross-linking pathways in MC3T3-E1 cells. *J Bone Miner Res*. (John Wiley & Sons, Ltd); 2004. p. 1349–55.

[46] Sacco AG, Cohen EE. Current Treatment Options for Recurrent or Metastatic Head and Neck Squamous Cell Carcinoma. *J. Clin. Oncol.* 2015;**33**:3305–13.

[47] Sada M, Ohuchida K, Horioka K, Okumura T, Moriyama T, Miyasaka Y, Ohtsuka T, Mizumoto K, Oda Y, Nakamura M. Hypoxic stellate cells of pancreatic cancer stroma regulate extracellular matrix fiber organization and cancer cell motility. *Cancer Letters* 2016;**372**:210–18.

[48] Saito T, Uzawa K, Terajima M, Shiiba M, Amelio AL, Tanzawa H, Yamauchi M. Aberrant Collagen Cross-linking in Human Oral Squamous Cell Carcinoma. *J. Dent. Res.* 2019:002203451982871.

[49] Schaub FX, Reza MS, Flaveny CA, Li W, Musicant AM, Hoxha S, Guo M, Cleveland JL, Amelio AL. Fluorophore-NanoLuc BRET Reporters Enable Sensitive In Vivo Optical Imaging and Flow Cytometry for Monitoring Tumorigenesis. *Cancer Res* 2015;**75**:5023–33.

[50] Setargew YFI, Wyllie K, Grant RD, Chitty JL, Cox TR. Targeting Lysyl Oxidase Family Meditated Matrix Cross-Linking as an Anti-Stromal Therapy in Solid Tumours. *Cancers (Basel)* 2021;**13**:491.

[51] Siegel R, Ma J, Zou Z, Jemal A. Cancer statistics, 2014. *CA Cancer J. Clin.* 2014;**64**:9–29.

[52] Siegel RL, Miller KD, Fuchs HE, Jemal A. Cancer Statistics, 2021. *CA: a Cancer Journal for Clinicians* 2021;**71**:7–33.

[53] Sun Y, Vandenbriele C, Kauskot A, Verhamme P, Hoylaerts MF, Wright GJ. A Human Platelet Receptor Protein Microarray Identifies the High Affinity Immunoglobulin E Receptor Subunit α (FcεR1α) as an Activating Platelet Endothelium Aggregation Receptor 1 (PEAR1) Ligand. *Molecular & Cellular Proteomics: MCP* 2015;**14**:1265–74.

[54] Tauriello DVF, Palomo-Ponce S, Stork D, Berenguer-Llergo A, Badia-Ramentol J, Iglesias M, Sevillano M, Ibiza S, Cañellas A, Hernando-Momblona X. TGFβ drives immune evasion in genetically reconstituted colon cancer metastasis. *Nature* 2018;**554**:538–43.

[55] Tian C, Clauser KR, Öhlund D, Rickelt S, Huang Y, Gupta M, Mani DR, Carr SA, Tuveson DA, Hynes RO. Proteomic analyses of ECM during pancreatic ductal adenocarcinoma progression reveal different contributions by tumor and stromal cells. *Proc. Natl. Acad. Sci. U. S. A.* 2019;**116**:19609–18.

[56] Trackman PC. Lysyl Oxidase Isoforms and Potential Therapeutic Opportunities for Fibrosis and Cancer. *Expert Opin. Ther. Targets* 2016;**20**:935–45.

[57] Ueki Y, Saito K, Iioka H, Sakamoto I, Kanda Y, Sakaguchi M, Horii A, Kondo E. PLOD2 Is Essential to Functional Activation of Integrin β1 for Invasion/Metastasis in Head and Neck Squamous Cell Carcinomas. *iScience* 2020;**23**:100850.

[58] Uzawa K, Grzesik WJ, Nishiura T, Kuznetsov SA, Robey PG, Brenner DA, Yamauchi M. Differential expression of human lysyl hydroxylase genes, lysine hydroxylation, and cross-linking of type I collagen during osteoblastic differentiation in vitro. *J Bone Miner Res*. (John Wiley & Sons, Ltd); 1999. p. 1272–80.

[59] van der Slot AJ, Zuurmond A-M, Bardoel AFJ, Wijmenga C, Pruijs HEH, Sillence DO, Brinckmann J, Abraham DJ, Black CM, Verzijl N, et al. Identification of PLOD2 as telopeptide lysyl hydroxylase, an important enzyme in fibrosis. *The Journal of biological chemistry* 2003;**278**:40967–72.

[60] van der Slot AJ, Zuurmond A-M, van den Bogaerdt AJ, Ulrich MMW, Middelkoop E, Boers W, Karel Ronday H, DeGroot J, Huizinga TWJ, Bank RA. Increased formation of pyridinoline cross-links due to higher telopeptide lysyl hydroxylase levels is a general fibrotic phenomenon. *Matrix biology: journal of the International Society for Matrix Biology* 2004;**23**:251–7.

[61] van der Slot-Verhoeven AJ, van Dura EA, Attema J, Blauw B, DeGroot J, Huizinga TWJ, Zuurmond A-M, Bank RA. The type of collagen cross-link determines the reversibility of experimental skin fibrosis. *Biochimica et biophysica acta* 2005;**1740**:60–7.

[62] Yamauchi M, Barker TH, Gibbons DL, Kurie JM. The fibrotic tumor stroma. *J Clin Invest*. (American Society for Clinical Investigation); 2018. p. 16–25.

[63] Yamauchi M, Sricholpech M. Lysine post-translational modifications of collagen. *Essays Biochem* 2012;**52**:113–33.

[64] Yamauchi M, Taga Y, Hattori S, Shiiba M, Terajima M. Analysis of collagen and elastin cross-links. *Methods in Cell Biology* 2018;**143**:115–32.